Available online at www.sciencedirect.com
SCIENCE DIRECT®
Surface Science 583 (2005) 60–68
SURFACE SCIENCE
www.elsevier.com/locate/susc

First principles study of H_2S adsorption and dissociation on Fe(1 1 0)

D.E. Jiang [a], Emily A. Carter [a,b,*]

[a] Department of Chemistry and Biochemistry, P.O. Box 951569, University of California, Los Angeles, CA 90095-1569, USA
[b] Department of Mechanical and Aerospace Engineering, Princeton University, D404A Engineering Quadrangle, Princeton, NJ 08544-5263, USA

Received 26 January 2005; accepted for publication 15 March 2005
Available online 31 March 2005

Abstract

We report first principles density functional theory (DFT) results of H_2S and HS adsorption and dissociation on the Fe(1 1 0) surface. We investigate the site preference of H_2S, HS, and S on Fe(1 1 0). H_2S is found to weakly adsorb on either the short bridge (SB) or long bridge (LB) site of Fe(1 1 0), with a binding energy of no more than 0.50 eV. The diffusion barrier from the LB site to the SB site is found to be small (~0.10 eV). By contrast to H_2S, HS is predicted to be strongly chemisorbed on Fe(1 1 0), with the S atom in the LB site and the HS bond oriented perpendicular to the surface. Isolated S atoms also are predicted to bind strongly to the LB sites of Fe(1 1 0), where the SB is found to be a transition state for S surface hopping between neighboring LB sites. The minimum energy paths for H_2S and HS dehydrogenation involve rotating an H atom towards a nearby surface Fe atom, with the S–H bonds breaking on the top of one Fe atom. The barrier to break the first S–H bond in H_2S is low at 0.10 eV, and breaking the second S–H bond is barrierless, suggesting deposition of S on Fe(1 1 0) via H_2S is kinetically and thermodynamically facile.

Keywords: Density functional calculations; Adsorption; Iron; Hydrogen sulfide; Dissociation

1. Introduction

The reaction of hydrogen sulfide with iron is of great importance in many different fields. For example, in cosmology, the formation of iron sulfide in solar nebula via reaction of H_2S with surfaces of bulk Fe greatly affected the nature of the planets and other bodies formed later [1]. In metal

* Corresponding author. Address: Department of Mechanical and Aerospace Engineering, Princeton University, D404A Engineering Quadrangle, Princeton, NJ 08544-5263, USA. Tel.: +1 609 258 5391; fax: +1 609 258 5877.
E-mail address: eac@princeton.edu (E.A. Carter).

0039-6028/$ - see front matter © 2005 Elsevier B.V. All rights reserved.
doi:10.1016/j.susc.2005.03.023

corrosion, H_2S in the gas or solution phase can attack structural metals aggressively; sulfur itself can embrittle transition metals such as Fe [2]. Although some research has been devoted to understanding the sulfidation of Fe [3,4], little is known about the adsorption geometries and dissociation pathways of H_2S on Fe surfaces, which characterize the initial stage of S deposition. This is likely caused by the fast kinetics of H_2S dissociation on transition metals, which prohibits detailed mechanistic and structural characterization experimentally. In this work, we use first principles theory to examine the adsorption and dissociation of H_2S on Fe surfaces.

We summarize experimental findings briefly here. Polycrystalline iron films [3–7] have been used in most experimental studies of H_2S interaction with iron. Narayan et al. studied iron sulfidation by H_2S from 110 to 773 K [4] with X-ray photoelectron spectroscopy (XPS). Based on binding energy shifts of the S 2p level, they concluded that H_2S adsorption is molecular at 110 K, but dissociative from 190 K up to ambient temperatures. At $T > 423$ K, they found formation of FeS, where an initial nonstoichiometric form converts to the stoichiometric form with increased H_2S dosing. No direct evidence (such as high-resolution electron energy loss spectroscopy) was presented to confirm the molecular adsorption of H_2S at 110 K. Most other H_2S adsorption experiments on iron surfaces were performed at room temperature or above, where no molecular H_2S or HS were observed, indicating the ease of H_2S dissociation. For example, Kelemen and Kaldor studied [8] S deposition on Fe(1 1 0) by dissociative adsorption of H_2S at 150 °C, using low energy electron diffraction (LEED). They found that S first forms a p(2 × 2) pattern (0.25 monolayer, ML) and then a p(3 × 1) pattern (1/3 ML, saturation coverage). The S–Fe(1 1 0)-p(2 × 2) structure was also observed in another LEED experiment [9].

In our earlier work [10], we studied H_2S adsorption and dissociation on Fe(1 0 0), one of the low-Miller-index surfaces of Fe. We found that H_2S is weakly adsorbed on Fe(1 0 0) and that the first and second dehydrogenation steps have a similar barrier of ~0.25 eV. Fe(1 0 0) is more open than Fe(1 1 0), the closest-packed surface of Fe. Convention wisdom suggests that the dissociation barriers of H_2S on Fe(1 1 0) will be higher than those on Fe(1 0 0), which motivates the present study. In this work, we characterize the H_2S and HS adsorption sites and dissociation pathways on Fe(1 1 0) with periodic density functional theory (DFT). In fact, we show that the convention wisdom regarding the decreased activity of closed-packed surfaces is wrong in this case. Overall, our work elucidates the initial kinetics of H_2S attack. This may be helpful for designing sulfur-tolerant steels.

The rest of the paper is organized as follows. Calculational details are given in Section 2. Predictions of H_2S, HS, and S adsorption structures and binding energies are presented in Sections 3.1, 3.2 and 3.3, respectively. Predicted pathways for H_2S dissociation are given in Section 3.4 and for HS dissociation in Section 3.5. We summarize and conclude in Section 4.

2. Calculational details

We perform first-principles calculations based on spin-polarized density functional theory (DFT) [11,12]. The Vienna Ab Initio Simulation Package (VASP) [13,14] is used to solve the Kohn–Sham equations with periodic boundary conditions and a plane-wave basis set. Here we employ Blöchl's all-electron projector augmented wave (PAW) method [15] as implemented by Kresse and Joubert [16]. For the treatment of electron exchange and correlation, we use the generalized gradient approximation (GGA) of PBE [17].

We use a kinetic energy cutoff of 400 eV for all the calculations, which converges the total energy to ~1 meV/atom for the primitive cell of bulk Fe. The Monkhorst–Pack scheme [18] is used for the k-point sampling. The first order Methfessel–Paxton method [19] is used for the Fermi surface smearing, with a width of 0.1 eV in order to obtain accurate forces. Using a $15 \times 15 \times 15$ k-mesh, we obtain an equilibrium lattice constant (a_0 = 2.83 Å), bulk modulus (B = 174 GPa), and local magnetic moment (M = 2.20 μ_B) for ferromagnetic bcc Fe. The results agree very well with previous

PAW-GGA calculations and experiment (a_0 = 2.86 Å, B = 168 GPa, M = 2.22 μ_B) [20].

To model gaseous H_2S, HS, and S atom, we place a molecule or atom in a 10 Å cubic box. We perform a non-spin-polarized calculation for H_2S, but spin-polarized calculations for open-shell HS and S, where the valence electron configuration used for S atom is ground state triplet $(3p)^4$, approximately ^3P (spin-polarized DFT open-shell states are all slightly spin-contaminated). The molecular geometry, vibrational frequencies, and bond dissociation energies from our work are in good agreement with experiment, as reported earlier [10].

Fe(1 1 0) is the closest-packed surface of bcc Fe and is basically bulk-terminated, with very little relaxation and no reconstruction. To model the Fe(1 1 0) surface, we use a five-layer slab and a 12-Å vacuum layer, which we showed previously are sufficiently thick [21]. We put adsorbates on one side of the slab; this produces a small dipole due to the dipole of the molecular adsorbate itself, as well as charge transfer between the adsorbate and the metal surface, so an a posteriori dipole correction to the total energy was included (the magnitude of the correction is <0.08 eV/cell). Only the top two layers of the five substrate layers are allowed to relax, together with the adsorbate layer. The bottom three layers are kept fixed in bulk positions to represent the semi-infinite bulk crystal beneath the surface (allowing the middle layer of the substrate to relax only changes the total energy of the slab by ~5 meV.) When the maximum force acting on each of the relaxed atoms drops below 0.01 eV/Å, the structural relaxation is stopped.

In this work, we study only 0.25 ML adsorbate coverages. Experiments show that 1/3 ML is the saturation coverage for S on Fe(1 1 0) as a p(3 × 1) superstructure. However, no direct observation of H_2S or HS on Fe(1 1 0) are available. We chose 0.25 ML as a compromise between minimizing adsorbate–adsorbate interactions and being close to the coverage of the stable overlayer structure of S on Fe(1 1 0) from experiment. Coverage effects on adsorption, diffusion, and dissociation of H_2S on Fe(1 1 0) are left to future work. High-symmetry sites on Fe(1 1 0) are displayed in Fig. 1. We use a k-mesh of 4 × 4 × 1 for the p(2 × 2) Fe(1 1 0) cell,

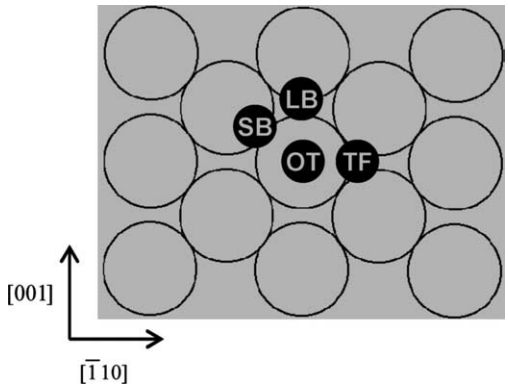

Fig. 1. High symmetry adsorption sites on Fe(1 1 0): OT = on-top, SB = short bridge, LB = long bridge and TF = threefold.

which converges the adsorption energy of H_2S to within 0.02 eV.

The climbing image nudged elastic band (CI-NEB) method [22,23] is used to locate the minimum energy paths (MEPs) and the transition states for H_2S diffusion, as well as H_2S and HS dissociation on Fe(1 1 0). An interpolated chain of configurations (images) between the initial and final positions are connected by springs and relaxed simultaneously to the MEP. With the climbing image scheme, the highest-energy image climbs uphill to the saddle point. We use the same force tolerance for the transition state search as that used for structural relaxations.

Vibrational frequencies of H_2S and HS on Fe(1 1 0) are determined by diagonalizing a finite difference construction of the Hessian matrix with displacements of 0.02 Å (only allowing H and S atoms to move). The natures of the relaxed adsorbate configurations and the saddle points found by the CI-NEB method are also checked in the same way we do vibrational frequency calculations.

3. Results and discussion

3.1. H_2S adsorption on Fe(1 1 0)

Previous experimental work of the sulfidation of Fe focused on thin films. No knowledge of H_2S geometry on Fe has been inferred, perhaps due to it fast dissociation kinetics above 190 K

[4]. To our knowledge, no low temperature characterization of the adsorbate structure has been attempted experimentally. H_2S can adopt many adsorption geometries on Fe(1 1 0), however we only explored the high-symmetry sites shown in Fig. 1. We started with four initial structures for the on-top (OT) site and two for each of the other sites. In two of the four structures for the OT site, the molecular plane of H_2S is parallel to the surface and the symmetry axis of H_2S is either parallel or perpendicular to [0 0 1] (see Fig. 1). In the other two initial structures for the OT site, the symmetry axis of H_2S is perpendicular to the surface and the H_2S plane is either parallel or perpendicular to [0 0 1]. In the initial structures for the other sites, the symmetry axis of H_2S is perpendicular to the surface. The lowest energy structures from the initial guesses for each of the sites are shown in Fig. 2 and their corresponding H_2S adsorption energies, geometries, and vibrational frequencies are displayed in Table 1. We see that H_2S is quite weakly adsorbed, with the short-bridge (SB) and the long-bridge (LB) sites almost degenerate at about -0.50 eV. The OT site is neither a local minimum nor a transition state, but a higher-order (rank-2) saddle point. We found that the threefold (TF) site is not stable for H_2S, with the adsorbate relaxing to the LB site after initially being placed at the TF site. For both LB and SB adsorption, the molecular plane and the symmetry axis of H_2S are perpendicular to the substrate surface, indicating an interaction between the two S lone electron pairs and the substrate Fe atoms. In another orientation we explored for the SB or LB site, the molecular plane is perpendicular to the one shown in Fig. 2(b) or (c), but its energy is 0.60 eV higher for the SB site and 0.20 eV higher for the LB site. Moreover, we found that if H_2S is initially oriented parallel to the surface at the LB or SB site, it dissociates.

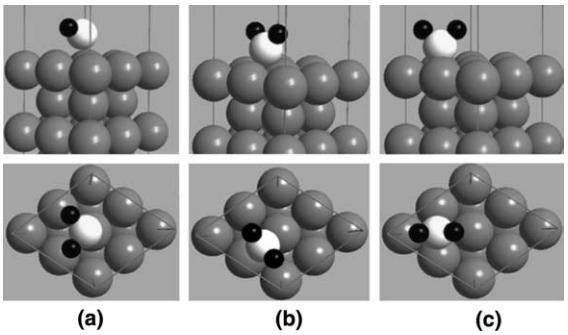

Fig. 2. Lowest energy structures of H_2S adsorbed on high symmetry adsites on Fe(1 1 0): (a) on-top; (b) short bridge; (c) long bridge. Upper panel is the side view, and lower panel is the top view. Fe atoms are in grey, S in white, and H in black. The same grey scale convention is used in all subsequent figures.

Because the interaction between H_2S and Fe(1 1 0) predicted from these DFT-PBE calculations is weak, we also evaluated H_2S adsorption on Fe(1 1 0) with the RPBE exchange-correlation functional [24] using PBE-optimized geometries. As usual, DFT-RPBE reduces the typical overbinding between adsorbates and the metal surface by DFT-PBE [24]. The resulting adsorption energies are only slightly negative (~ -0.15 eV) and very similar for all three sites (OT, LB, and SB), indicating the interaction between H_2S and Fe(1 1 0) is indeed weak. We caution that such weak interactions are not well described by conventional DFT-GGA theory.

At the SB site, the geometry of H_2S changes only slightly upon adsorption (slightly lengthened H–S bonds), but stretching frequencies are significantly softened. At the LB site, the softening of stretching frequencies is even more pronounced, with H–S bonds even longer than for adsorption on the SB site. By contrast, the H–S–H bond angle remains very similar to the gaseous H_2S value, with only a slight blue-shifting of the bending frequencies. Moreover, H_2S is closer to the Fe(1 1 0) surface in the LB site. All of these trends point to stronger interactions between H_2S and Fe at the LB site.

3.2. HS adsorption on Fe(1 1 0)

We find that the final structure of HS on Fe(1 1 0) depends strongly on the initial guess employed. Many initial guess structures resulted in dissociation of HS to H and S on Fe(1 1 0), indicating that HS is likely to be unstable on Fe(1 1 0). Fig. 3 shows the three high symmetry adsorption sites obtained for HS on Fe(1 1 0) and Table 2 displays their corresponding binding energies, vibrational frequencies, and geometries. Only the LB

Table 1
Adsorption energy [$E_{ad} = E(H_2S/Fe\text{-slab}) - E(Fe\text{-slab}) - E(H_2S)$] of H_2S on Fe(1 1 0), H–S bond length (r_{S-H}), smallest Fe–S distance (d_{Fe-S}), the height of S atom over Fe(1 1 0) (h), H–S–H bond angle (θ_{HSH}), and H_2S vibrational frequencies, including the asymmetric stretch (ω_a), the symmetric stretch (ω_s), the bend (ω_b), the frustrated rotations (ω_r), the adsorbate–substrate stretch (ω_{Fe-S}), and the two frustrated translations (ω_t)

Site	OT	SB	LB
E_{ad} (eV)	−0.39 (hos)	−0.50 (min)	−0.49 (min)
r_{S-H} (Å)	1.363	1.376	1.385
d_{Fe-S} (Å)	2.226	2.245	2.255
h (Å)	2.285	1.902	1.727
θ_{HSH} (°)	93.9	91.7	89.7
ω_a (cm^{-1})	2466	2338	2284
ω_s (cm^{-1})	2443	2282	2165
ω_b (cm^{-1})	1195	1195	1221
ω_r (cm^{-1})	231, 367i, 423	370, 381, 414	337, 435, 454
ω_{Fe-S} (cm^{-1})	177	219	211
ω_t (cm^{-1})	47i, 71	113, 163	70, 129

The nature of the critical point is given in parentheses (min = minimum and hos = higher order saddle point) and imaginary frequencies are denoted by "i" after the frequency magnitude. DFT-PAW-GGA (PBE) predicts (this work) that isolated H_2S has $r_{S-H} = 1.349$ Å, $\omega_a = 2618\ cm^{-1}$, $\omega_s = 2607\ cm^{-1}$, $\omega_b = 1151\ cm^{-1}$, and $\theta_{HSH} = 91.6°$.

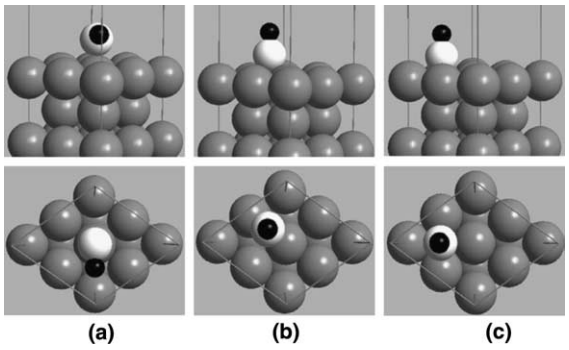

Fig. 3. Lowest energy structures of HS adsorbed on high symmetry adsites on Fe(1 1 0): (a) on-top; (b) short bridge; (c) long bridge. Upper panel is the side view, and lower panel is the top view.

site is a local minimum, with HS strongly chemisorbed on Fe(1 1 0) and the HS bond pointing along the surface normal. By contrast, both the OT and SB sites are rank-2 saddle points. We observe a softening of the H–S stretching frequency upon adsorption, consistent with the lengthening and likely weakening of the H–S bond.

Fig. 4 displays an electron density difference plot for HS at the LB site. One can see that the rearrangement of electron density reflects the C_{2v} symmetry of the adsorbate structure. Electron density is depleted from under the S atom, from the two sides of the S atom facing the two closer Fe atoms (B-type Fe atom in Fig. 4, $d_{Fe-S} = 2.21$ Å), and also from those two Fe atoms, while electron density accumulates on the other two sides of the S atom facing the two farther Fe atoms (A-type Fe in Fig. 4, $d_{Fe-S} = 2.46$ Å). The accumulated electron density appears to be in an S p-orbital, suggesting charge rearrangement to render the S p-orbitals in HS equally populated. In the extreme limit, the depletion of charge from Fe would produce $HS^-_{(a)}$, which has filled p-orbitals that would prefer a perpendicular adsorption structure (as found here) to optimize electron back-donation toward the Fe surface.

3.3. S adsorption on Fe(1 1 0)

The adsorption of S on Fe(1 1 0) at 0.25 ML can cause a mild reconstruction of the metal surface, and S is found to reside on the LB site, as shown by LEED [9]. A recent DFT-USPP-GGA (PW91) study [25] by Spencer et al. reported the structural details of S–Fe(1 1 0)-p(2 × 2) and confirmed the LB site preference by LEED. Our study also shows that S is strongly chemisorbed on the LB site, with the LB site as the only minimum (Table 3). The SB site is a transition state for S diffusion on Fe(1 1 0), with a barrier of

Table 2
Adsorption energy [$E_{ad} = E_{HS/Fe\text{-}slab} - E_{Fe\text{-}slab} - E_{HS}$] of HS on Fe(110), H–S bond length (r_{S-H}), smallest Fe–S distance (d), the height of S atom over Fe(110) (h), tilt angle of H–S bond axis with respect to the surface normal (θ), and HS vibrational frequencies, including the stretch (ω_s), the frustrated rotations (ω_r), the adsorbate–substrate stretch (ω_{Fe-S}), and the two frustrated translations (ω_t)

Site	OT	SB	LB
E_{ad} (eV)	−2.855 (hos)	−2.877 (hos)	−3.467 (min)
r_{H-S} (Å)	1.359	1.371	1.373
d_{Fe-S} (Å)	2.135	2.188	2.206
h (Å)	2.194	1.726	1.526
θ (°)	73.7	0	0
ω_s (cm^{-1})	2498	2368	2355
ω_r (cm^{-1})	127, 577	317, 389*i*	213, 431
ω_{Fe-S} (cm^{-1})	291	268	275
ω_t (cm^{-1})	50i, 78i	86, 97i	122, 221

The nature of the critical point is given in parentheses (min = minimum, and hos = higher order saddle point). DFT-PAW-GGA (PBE) predicts (this work) that isolated HS has $r_{S-H} = 1.354$ Å and $\omega_s = 2616\ cm^{-1}$.

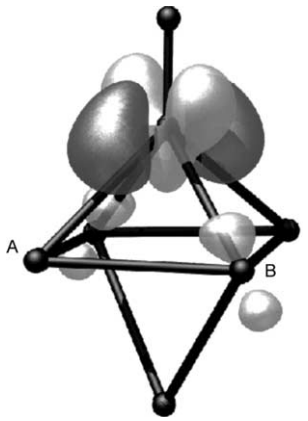

Fig. 4. Isosurface plot of the electron density difference, $\Delta\rho$, for HS/Fe(110) in the long-bridge site. Solid black balls represent atoms: the top one is H, the one below H is S, and the atoms below S are Fe atoms. The isosurface value is at $-0.05\ e/Å^3$ for the light grey surface and at $0.05\ e/Å^3$ for the dark grey surface. Negative $\Delta\rho$ indicates loss of electron density upon binding.

0.52 eV. By contrast, the on-top site is a rank-2 saddle point.

Our theoretical predictions of the Fe–S distances and the height of S atoms over the substrate are close to the DFT-GGA results by Spencer et al. [9]. Moreover, we also found a buckling of the surface and subsurface substrate layers as Spencer et al. did in their study. However, this degree of freedom was not included in the models of Shih et al.'s LEED study [9]. This may account for the rather large discrepancy between DFT-GGA and experiment regarding the height of S atom above the substrate surface (Table 3).

3.4. H_2S dissociation on Fe(110)

As mentioned above, we use the nudged elastic band (NEB) method to locate the minimum energy path for H_2S dissociation to HS and H. The NEB method requires that the initial and final states of the transition be specified beforehand. We consider first the dehydrogenation of H_2S to HS and H. In the initial state H_2S will reside either on the LB site or the SB site, since they are almost degenerate. We have examined the diffusion from the LB site to the SB site, and the barrier is small (~0.11 eV). In Section 3.1, we showed that the structure of H_2S changes more upon adsorption at the LB site than the SB site, so we begin with the LB site since it may be that H_2S is more activated at this site. Next we need to know where HS prefers to be in the presence of H (for the final state). Our earlier study of H/Fe(110) [21] showed that H always prefers the TF site for the coverage of 0.11–1.0 ML. We tried several combinations of HS in the LB site and H in the nearby TF site. We found only one stable configuration with these two species close to each other. In all the other cases, HS lost its hydrogen, just as we found for the many initial structures of the isolated HS group on Fe(110). This indicates again that HS is rather unstable on Fe(110).

Fig. 5 shows the minimum energy path of the dehydrogenation of H_2S to HS and H starting with

Table 3
Adsorption energy [$E_{ad} = E_{S/Fe\text{-}slab} - E_{Fe\text{-}slab} - E_S$] of S atom on Fe(1 1 0), the smallest Fe–S distance ($d_{Fe—S}$), the height of S atom over Fe(1 1 0) (h), and the S vibrational frequencies, including the adsorbate–substrate stretch ($\omega_{Fe—S}$) and the two frustrated translations (ω_t)

Site	OT[a]	SB[a]	LB[a]	LB[b]	Experiment[c]
E_{ad} (eV)	−4.408 (hos)	−5.271 (ts)	−5.788 (min)	–	–
$d_{Fe—S}$ (Å)	2.038	2.144	2.180	2.19	2.17
h (Å)	1.917	1.655	1.526	1.567	1.43
$\omega_{Fe—S}$ (cm^{-1})	396	353	325	–	–
ω_t (cm^{-1})	117i, 130i	125i, 231	111, 257	–	–

The nature of the critical point is given in parentheses (min = minimum, ts = transition state, and hos = higher order saddle point).
[a] This work.
[b] Ref. [25].
[c] Ref. [9].

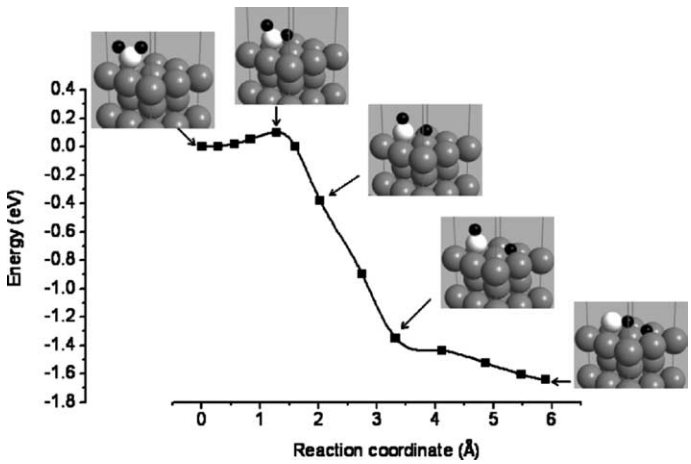

Fig. 5. DFT-GGA minimum energy path for H_2S dissociation on Fe(1 1 0).

H_2S on the LB site. The structures for the initial and final states, together with several intermediate structures, are also shown in Fig. 5. We predict that H_2S breaks one H–S bond by rotating one H atom towards a nearby surface Fe atom and the H–S bond dissociates over that Fe atom. The dissociation barrier is 0.10 eV, indicating the ease of breaking the first H–S bond of H_2S on Fe(1 1 0). At the transition state, the length of the breaking H–S bond is 1.45 Å, only 0.07 Å longer than the initial state. After the transition state, one H atom breaks away and moves to the TF site with a ~1.40 eV energy drop. Then the system descends through a flat step to reach the final state with an energy drop of 0.20 eV, which corresponds to bending of the HS group towards H. In the final state, the HS group is stabilized by ~0.30 eV by the presence of the nearby H atom, compared to isolated $HS_{(a)}$. Despite this, H–S bond is still significantly lengthened at 1.49 Å. We found that HS will spontaneously dissociate to H and S over the opposite Fe atom if the HS group rotates away from H.

Four Fe atoms coordinate around S when H_2S resides at the LB site, with two of them farther away from the S atom than the other two. Fig. 5 shows that H_2S breaks its first H–S bond on one of the two more distant Fe atoms, with a barrier of 0.10 eV. We also examined dissociation of H_2S on one of the two closer Fe atoms. The barrier is 0.11 eV, almost the same as the former. This indicates that H_2S can break its first H–S bond on any of the four Fe atoms coordinated around S with a very low barrier. In our earlier study of

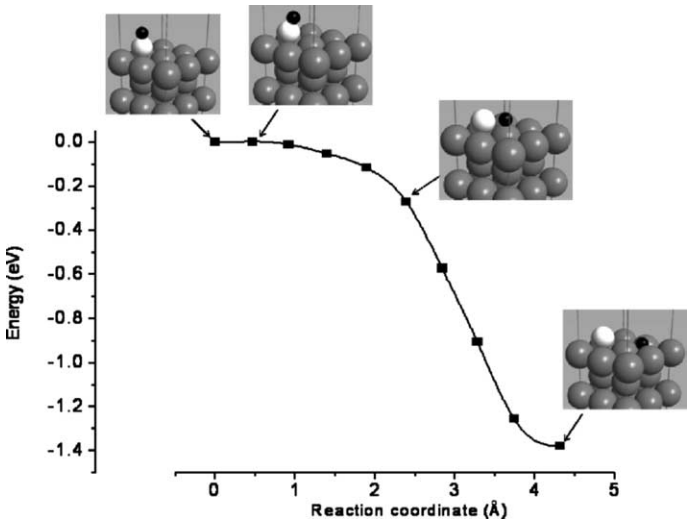

Fig. 6. DFT-GGA minimum energy path for HS dissociation on Fe(1 1 0).

H_2S dissociation on Fe(1 0 0), we also found that H_2S breaks its H–S bonds on top of one Fe atom coordinated to S [10], again with a relatively low barrier of 0.25 eV.

3.5. HS dissociation on Fe(1 1 0)

From the above discussion, we already observed that HS is at best metastable on Fe(1 1 0). To further confirm this finding, we examine the dehydrogenation of HS on Fe(1 1 0) in the absence of H. We found an MEP (Fig. 6), which is similar to the first dehydrogenation step of H_2S. However, the barrier here is much smaller, basically zero (1 meV). At the ''transition state'', the HS axis is rotated ~19° toward the surface compared with the initial state and we see that the potential energy surface (PES) is very flat from the initial state to the ''transition state''. Such a flat PES indicates that, within the inherent errors of DFT-GGA, we essentially have no barrier, no transition state, and simply a spontaneous exothermic reaction. The large exothermicity provides the driving force for spontaneous dissociation of HS.

In our earlier work, we examined H_2S dissociation on the more open, but similarly stable, Fe(1 0 0) surface. Conventional wisdom might suggest that dissociation of H_2S on the less highly coordinated Fe(1 0 0) surface would have a lower barrier. Instead, we found that the barriers to break the first and second S–H bonds in H_2S on Fe(1 0 0) are about the same, ~0.25 eV, and non-trivially higher than those on Fe(1 1 0).

4. Conclusions

Using periodic density functional theory within the all-electron projector augmented wave formalism and the generalized-gradient approximation to electron exchange and correlation, we have studied H_2S, HS, and S adsorption, H_2S and S diffusion, and H_2S and HS dissociation on Fe(1 1 0). We find that H_2S is weakly molecularly adsorbed on either the long bridge (LB) or short bridge (SB) site of Fe(1 1 0), with the molecular plane oriented along the surface normal. The adsorption of H_2S in a bridge site is exothermic by 0.50 eV. Adsorption at an on-top site is not a local minimum for H_2S on Fe(1 1 0), but a higher order saddle point. This is likely due to the interaction of the two H_2S lone pairs, which drive H_2S to higher coordination sites. The diffusion barrier between the LB and the SB sites is predicted to be only ~0.10 eV. By contrast with H_2S, HS is strongly chemisorbed on Fe(1 1 0). The only stable configuration of HS on Fe(1 1 0) has S in the LB site and the HS bond upright, with a binding energy of 3.47 eV. At this

adsorption configuration, the two S p-orbitals of HS redistribute charge to be equally occupied in order to interact better with Fe(1 1 0). Lastly, we find that S atom strongly binds to the LB site of Fe(1 1 0). The SB site serves as a transition state with a barrier of 0.52 eV for diffusion between two neighboring LB sites for S/Fe(1 1 0).

With the climbing-image nudged elastic band method, we obtained the minimum energy paths for H_2S and HS dehydrogenation on Fe(1 1 0). Starting from the LB site, we predict that H_2S loses one H atom by rotating the molecule to orient the H atom towards one of Fe atoms coordinated to the S atom. The dissociation barrier is very small, 0.10 eV, independent of which type of Fe atom is involved. After the transition state, the H atom first moves from the on-top site to the three-fold site, and then the HS group rotates towards the breaking-away H atom and is stabilized in a lying-down configuration. If the HS group rotates away from the H atom, the HS group immediately dehydrogenates further to S and H, due to the larger exothermicity of this reaction. In the absence of H, HS breaks its bond in exactly the same way that H_2S loses its first H, but with essentially no barrier. Our present work shows that H_2S loses its first H with a barrier of 0.10 eV and its second H effortlessly on Fe(1 1 0); our earlier work for H_2S/Fe(1 0 0) indicated similarly high reactivity, with only slightly higher dissociation barriers ($\sim$0.25 eV [10]). Since the (1 1 0) and (1 0 0) surfaces are the most stable surfaces of Fe, they tend to be preferentially exposed. Our work therefore implies that H_2S will attack polycrystalline iron (and steel) surfaces in a much faster manner than will other deleterious gases such as CO, where dissociation barriers are considerably higher [26,27].

Acknowledgement

This work was supported by the Army Research Office. We thank the Maui High Performance Computing Center and the NAVO Major Shared Resources Center for CPU time.

References

[1] D.S. Lauretta, K. Lodders, B. Fegley Jr., Science 277 (1997) 358.
[2] C.L. Briant, K. Sieradzki, Phys. Rev. Lett. 63 (1989) 2156.
[3] D.S. Lauretta, D.T. Kremser, B. Fegley Jr., ICARUS 122 (1996) 288.
[4] P.B.V. Narayan, J.W. Anderegg, C.W. Chen, J. Electron Spectrosc. Relat. Phenom. 27 (1982) 233.
[5] D.R. Baer, M.T. Thomas, R.H. Jones, Metall. Trans. A: Phys. Metall. Mater. Sci. A 15 (1984) 853.
[6] M.R. Shanabarger, R.D. Moorhead, Surf. Sci. 365 (1996) 614.
[7] H. Cabibil, J.A. Kelber, Surf. Sci. 373 (1997) 257.
[8] S.R. Kelemen, A. Kaldor, J. Chem. Phys. 75 (1981) 1530.
[9] H.D. Shih, F. Jona, D.W. Jepsen, P.M. Marcus, Phys. Rev. Lett. 46 (1981) 731.
[10] D.E. Jiang, E.A. Carter, J. Phys. Chem. B 108 (2004) 19140.
[11] P. Hohenberg, W. Kohn, Phys. Rev. B 136 (1964) B864.
[12] W. Kohn, L.J. Sham, Phys. Rev. A 140 (1965) 1133.
[13] G. Kresse, J. Furthmüller, Phys. Rev. B 54 (1996) 11169.
[14] G. Kresse, J. Furthmüller, Comput. Mater. Sci. 6 (1996) 15.
[15] P.E. Blöchl, Phys. Rev. B 50 (1994) 17953.
[16] G. Kresse, D. Joubert, Phys. Rev. B 59 (1999) 1758.
[17] J.P. Perdew, K. Burke, M. Ernzerhof, Phys. Rev. Lett. 77 (1996) 3865.
[18] H.J. Monkhorst, J.D. Pack, Phys. Rev. B 13 (1976) 5188.
[19] M. Methfessel, A.T. Paxton, Phys. Rev. B 40 (1989) 3616.
[20] D.E. Jiang, E.A. Carter, Phys. Rev. B. 67 (2003) 214103.
[21] D.E. Jiang, E.A. Carter, Surf. Sci. 547 (2003) 85.
[22] H. Jónsson, G. Mills, K.W. Jacobsen, Classical and quantum dynamics in condensed phase simulations, in: B.J. Berne, G. Ciccotti, D.F. Coker (Eds.), Classical and Quantum Dynamics in Condensed Phase Simulations, World Scientific, Singapore, 1998, p. 385.
[23] G. Henkelman, B.P. Uberuaga, H. Jónsson, J. Chem. Phys. 113 (2000) 9901.
[24] B. Hammer, L.B. Hansen, J.K. Nørskov, Phys. Rev. B 59 (1999) 7413.
[25] M.J.S. Spencer, A. Hung, I.K. Snook, I. Yarovsky, Surf. Sci. 540 (2003) 420.
[26] D.C. Sorescu, D.L. Thompson, M.M. Hurley, C.F. Chabalowski, Phys. Rev. B 66 (2002) 035416.
[27] D.E. Jiang, E.A. Carter, Surf. Sci. 570 (2004) 167.